Liquid Crystals
Publication details, including instructions for authors and subscription information:
http://www.informaworld.com/smpp/title~content=t713926090

Computer simulation of dynamics and morphology of discotic mesophases in extensional flows

Arvinder P. Singh[a]; Alejandro D. Rey[a]
[a] Department of Chemical Engineering, McGill University, Montreal, Quebec, Canada

To cite this Article Singh, Arvinder P. and Rey, Alejandro D.(1995) 'Computer simulation of dynamics and morphology of discotic mesophases in extensional flows', Liquid Crystals, 18: 2, 219 — 230
To link to this Article: DOI: 10.1080/02678299508036617
URL: http://dx.doi.org/10.1080/02678299508036617

LIQUID CRYSTALS, 1995, VOL. 18, NO. 2, 219–230

Computer simulation of dynamics and morphology of discotic mesophases in extensional flows

by ARVINDER P. SINGH and ALEJANDRO D. REY*

Department of Chemical Engineering, McGill University, Montreal, Quebec, H3A 2A7, Canada

(*Received 22 February 1994; accepted 5 March 1994*)

A previously presented model is used to simulate the dynamics and microstructure of spatially invariant uniaxial discotic nematic liquid crystals in isothermal, incompressible, irrotational, extensional (shear-free or elongational) flows. Numerical and analytical solutions of the director **n** and alignment S are presented for given uniaxial extensional, equi-biaxial extensional and planar extensional start-up flows. The unit sphere description of the director is used to discuss and analyse the sensitivity of the director trajectories and the alignment relaxation to the initial conditions ($\mathbf{n}_o$, S_o), to the alignment Deborah number (De), and to the type of flow. The numerical results are used to characterize the relaxation of the tensor order parameter **Q** and to compute the steady flow birefringence. The various flows are classified according to their orienting strength and alignment strength, and according to whether they generate geodesic (shortest path) director orbits. Equi-biaxial extensional and planar extensional flows are found to be strongly orienting and strongly aligning flows, while uniaxial extensional flow is a weakly orienting and weakly aligning flow. The number of strain units required to achieve steady state are shown to depend on whether the flow is geodesic (uniaxial extensional and equi-biaxial extensional flows) or not (planar extensional flow).

1. Introduction

Carbonaceous mesophases are an important class of naturally occurring discotic nematic liquid crystals [1–3]. These mesophases are formed by condensation of aromatic rings and tend to adopt a uniaxial discotic nematic phase (N_d [4, 5], with the unit normals to the disc-like molecules more or less aligned along a common direction (see figure 2(*b*)), represented by the director **n**; in this paper we use **n** and orientation interchangeably. Carbonaceous mesophases can be spun into stiff and strong (high performance) fibres [2, 3, 6], and understanding their flow behaviour is of practical utility.

Many industrial materials processing methods, such as the moulding of polymers, are designed with the objectives that the alignment and orientation introduced during the deformation and forming stages are controlled [7]. The process choices are based on these two independent qualities of the flow, its orienting and aligning strength, which also form the basis for polymer flow classifications [8]. Although such classification has not been developed for discotic mesophase fluids, it certainly can provide useful guidelines on the dependence of orientation and alignment on flow type. In this respect extensional flows, such as spinning flows, seem to be the most relevant to processing discotic mesophase fluids.

*Author for correspondence.

Previous work [9–13] on the flow properties of uniaxial discotic nematics assumed that the scalar order parameter S (alignment) remains unaffected by the flow, and were based on the Leslie–Ericksen (L–E) theory [14, 15] for uniaxial nematics. The important differences in sign and magnitude of the material parameters corresponding to uniaxial rod-like and discotic nematics follow from the fact that rod-like nematics orient their longest molecular dimension along the director while disc-like nematics orient their shortest molecular dimension along the director. As is well known, the orienting properties of uniaxial nematics during shear flow are governed by the sign and magnitude of the tumbling (reactive) parameter λ: for aligning (non-aligning) rods $\lambda > 1$ $(0 < \lambda < 1)$, and for aligning (non-aligning) discs $\lambda < -1$ $(-1 < \lambda < 0)$; the tumbling parameter λ is given by the negative ratio of the irrotational torque coefficient (γ_2) and the rotational viscosities (γ_1), and represents the coefficient of the ratio of strain to vorticity torques acting on the director **n**. Previous work [10, 11] focused on the orienting properties of aligning uniaxial discotic nematics in steady shear, and it was found that shear orients the director in the shear plane and at a steady angle θ, lying in the $90° \leq \theta \leq 135°$ sector with respect to the flow direction. In steady uniaxial extensional flows, the orienting behaviour of uniaxial nematics is again determined by the sign of λ: when $\lambda > 0$ the director aligns along the stretching

0267-8292/95 $10·00

(extension) direction, and when $\lambda<0$ the director aligns somewhere in the compression plane, orthogonal to the stretching direction [13].

For materials of larger molecular weights the coupling between the director and the scalar order parameter should be retained [16]. This coupling introduces additional nonlinearities through the dependence of the generalized Leslie coefficients on the scalar order parameter, as shown in various works [16–21]. In a previous work [22], the authors developed from variational principles a model that takes into account variable alignment in discotic nematics, and applied it to uniaxial extensional flow. It was found that the director trajectories on the unit sphere ($\mathbf{n}.\mathbf{n}=1$) follow a geodesic flow from the initial orientation to the compressional plane, and that the alignment relaxation was sensitive to the initial orientation, to the extension rate, and to the nematic potential that controls the magnitude of S in the absence of flow. The sensitivity to initial conditions, typical of geodesic flows, was shown to be the cause for the loss of predictability that occurs when the initial orientation lies along the extension axis of the flow.

Our main objective in this work is to establish the relevant qualitative features that describe the relations between extensional deformation inputs and orientation and alignment responses, in a model discotic nematic liquid crystal, and to use these results to formulate a practical flow classification of various extensional flows. In the present paper the phenomenological parameters of the particular model discotic nematic liquid crystal chosen for study are not fitted to those of any existing real material, and their choice is based on previous results [22]. The particular objectives of this paper are:

(1) To characterize the sensitivity of the director paths to the compressional axis or compressional plane, to the initial conditions, to the extension rate, and to the flow type, by using numerical simulation;
(2) To characterize the alignment relaxation along the director paths, to the initial conditions, to the extension rate, and to the flow type by using numerical simulation;
(3) To determine the geometry of the director trajectories to the compression axis or compressional plane, and to classify various extensional flows as geodesic or non-geodesic flows;
(4) To provide a general classification for extensional flows according to the magnitude of their alignment strength and orientation strength.

The organization of this paper is as follows. In § 2 we define the coordinate system and the state variables, present the governing equations, and briefly present the elements of the unit sphere description used to discuss and classify the numerical solutions. A brief description of the numerical method used to integrate the governing equations is presented. In § 3 we present, discuss, and classify the solution vector, consisting of the time dependent director and alignment fields, obtained from numerical integration and analytical solutions of the governing equations. Typical computations of the tensor order parameter relaxation and steady flow birefringence are presented. Overall classifications according to trajectory geometry of the director on the unit sphere, alignment strength, and orientation strength are given.

2. Governing equations

2.1. *Definitions of coordinates, kinematics, orientation and alignment*

In this paper we study the temporal and spatiall invariant microstructural response of a model uniaxial discotic nematic, subjected at time $t=0$, to a range of extensional flows of constant extension rate $\dot{\varepsilon}$. In this paper the adopted fluid flow terminology is that of Bird *et al.* [23]. Due to their prevalence in applications here we emphasize the three representative extensional flows: uniaxial extensional flow, equi-biaxial extensional flow, and planar extensional flow, but whenever possible allow for further generalizations by introducing representative parameters, as given in [23]. In the rest of this paper equi-biaxial extensional flow is referred to as biaxial extensional flow. Figure 1 shows the deformation of a cube of discotic nematic liquid crystal subjected at time $t=0$ to: (*a*) uniaxial extensional flow (UE), (*b*) biaxial extensional flow (BE), and (*c*) planar extensional flow (PE). We note that the word uniaxial in uniaxial extensional flow and biaxial in biaxial extensional flow refer to the number of extension (stretching or pulling) directions; these irrotational flows are three dimensional. Equi-biaxial extensional flow is kinematically the inverse of uniaxial extensional flow. On the other hand, planar extensional flows, also known as pure shear [24, 25] or strip biaxial flows, are irrotational two-dimensional flows, where the deformation characterized by an extension direction and an orthogonal contraction director occurs on a plane. In planar extensional flow the stream lines are a family of rectangular hyperbola whose centre is a stagnation (saddle) point [25].

An experimental set-up to generate a uniaxial extensional flow is to pull a cylindrical sample from two opposite ends at a rate that increases exponentially with time; in figure 1 the sketch representing uniaxial extension (UE), using rectangular coordinates, shows the extension direction along the x axis while the contraction directions are along the y and z axes. A way to generate a biaxial extensional flow is to stretch a thin sheet of material in two orthogonal directions simultaneously at an equal rate, with a corresponding decrease in the sheet

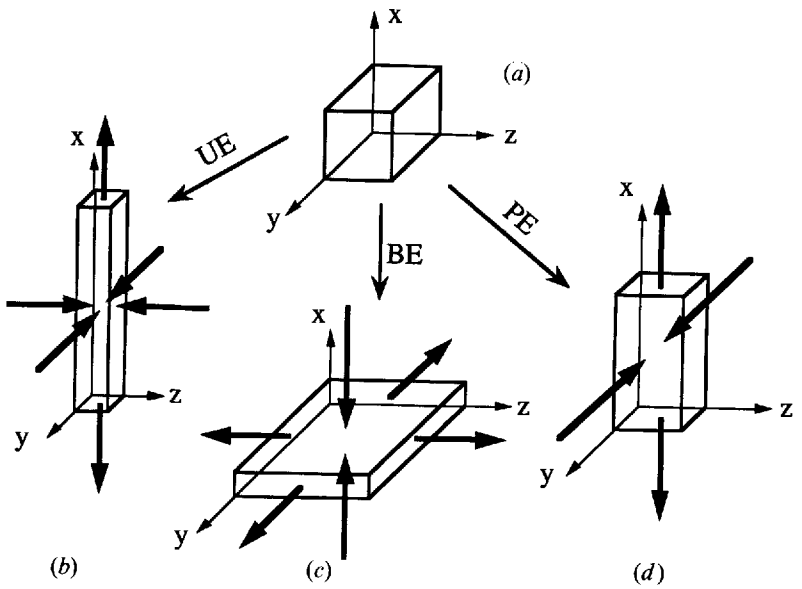

Figure 1. Deformation of (*a*) unit cube of material at time $t>0$ submitted to (*b*) uniaxial extension flow (UE), (*c*) biaxial extensional flow (BE), and planar extensional flow (PE). The velocity components for these flows are given in equation (10). In uniaxial extension (UE) flow, the x axis is the extension direction and the y and z axes are the directions of compression; this flow is an irrotational 3D flow. In biaxial extensional (BE) flow the y and z axes are the extension directions and the x axis is the compression direction; this three-dimensional irrotational flow is kinematically the inverse of uniaxial extension. In planar extension, the extension direction is along the x axis, the contraction direction is along the y axis, while no motion occurs along the z axis; planar extensional flow is a two-dimensional (planar) irrotational flow.

thickness. An approximation to this flow is found in lubrication squeeze-film flow and during the inflation of a balloon; in figure 1 the sketch representing biaxial extension (BE), using rectangular coordinates, shows the two extension directions along the y and z axes while the contraction direction is along the x axis. Planar extensional flow is equivalent to stretching a flat thin sheet of fluid in one direction, with a corresponding contraction in an orthogonal direction, but with no motion in the third direction; in figure 1 the sketch representing planar extension (PE), using rectangular coordinates, shows the extension direction along the x axis, the contraction direction along the y axis, while along the z axis no motion occurs. An experimental generation of an approximate planar extensional flow is the four-roll mill flow, where four long cylinders of equal radii, placed along the four corners of a square are set to rotate with equal magnitude but with directions opposite to the two nearest neighbours. The resulting essentially two-dimensional irrotational flow generates a family of rectangular hyperbolic stream lines, with a stagnation point at the centre of the square.

The microstructure of the model nematic considered here is characterized by the uniaxial tensor order parameter $Q_{ij}(t)$ [15]

$$Q_{ij}=S(n_in_j-\delta_{ij}/3), \qquad (1\,a)$$

where the following restrictions apply:

$$Q_{ij}=Q_{ji};\quad Q_{ii}=0;\quad -1/2\le S\le 1;\quad n_in_i=1 \qquad (1\,b)$$

and δ_{ij} is the unit tensor. The magnitude of the scalar order parameter S is a measure of the molecular alignment along the director $\mathbf{n}$, and its magnitude is given by $S=3(n_iQ_{ij}n_j)/2$. Equation (1 *a*) gives a proper description of the macroscopic order in a discotic nematic phase if we identify the director as the average orientation of the unit normals to the molecular discs; see figure 2 (*b*); as explained in [26], with this identification, S is positive for both rod-like and disc-like uniaxial nematic liquid crystals, and no further distinction is required in this paper since rods are not considered here. Since extensional flows will not induce negative values of the scalar order parameter S we further restrict its variation to the positive unit interval, $0\le S\le 1$ [26].

To enforce the unit length constraint $\mathbf{n}.\mathbf{n}=1$ and to visualize the director orbits on the unit sphere, we parametrize the director with

$$\mathbf{n}=(n_x, n_y, n_z)=(\cos\phi, \sin\phi\cos\theta, \sin\phi\sin\theta), \quad (2)$$

where θ ($0\le\theta\le 2\pi$) is the azimuthal angle and ϕ ($0\le\phi\le\pi$) is the polar angle, see figure 2 (*a*). The north pole of the sphere is located at $\phi=0$, the south pole at $\phi=\pi$, and the equator at $(\theta,\phi)=([0,2\pi], \pm\pi/2)$.

In the unit sphere description [27–29] the director tip,

in the presence of flow, defines a trajectory $O(\mathbf{n}_0)$ on the surface of the sphere

$$O(\mathbf{n}_0)=\{\mathbf{n}\in\Omega^2;\ \mathbf{n}=\mathbf{n}(t,\mathbf{n}_0),\ r\in P^+\}, \tag{3}$$

where $\mathbf{n}_0=\mathbf{n}$ $(t=0)$, Ω^2 denotes the surface of the unit sphere and P^+ the positive reals. To characterize some of the director orbits $O(\mathbf{n}_0)$ of interest we need to define some unique trajectories such as geodesics and meridians. A geodesic G is the shortest arc connecting two points on the sphere, and is given by [30]

$$\sin(N_2)\cos\phi-(\cos N_2)\sin\phi\cos\theta-\frac{\sin\phi\sin\theta}{\sqrt{(1/N_1^2-1)}}=0 \tag{4}$$

where N_1 and N_2 are constants that depend on two points belonging to G; the geodesic or great circle, is the intersection of the sphere with the plane containing the given points and the centre of the sphere. When the two points are the poles $(N_2=\pi)$ the degenerate geodesics are the meridians M, which in terms of (θ,ϕ) and the director components $(n_i,\ i=x,\ y,\ z)$, are given by [30]

$$\tan\theta=1/d_1;\quad d_1^2=1/(N_1^{-2}-1);\quad 0\le\phi\le\pi \tag{5a, b, c}$$

and

$$n_y=d_1n_z;\quad -1\le n_y\le 1;\quad -1\le n_z\le 1, \tag{6a, b, c}$$

where d_1 $(-\infty<d_1<\infty)$ is a constant whose numerical value defines a particular meridian; a family of meridians, is shown, by the full lines, in figure 2 (*a*).

To characterize the initial relaxation of the alignment as the director traverses the surface of the sphere, we divide the sphere into different characteristic regions, as shown in figure 5, by the R^+ and R^- regions. In irrotational extensional flows, the only flow effect on the orientation and alignment is due to the symmetric part of the velocity gradient tensor (v_{ij}), known as the rate of strain tensor and here denoted by **A**, and whose **ij**th and **ji**th components are given by $A_{ij}=A_{ji}=(v_{i,j}+v_{j,i})/2$. An important observation, used below to classify the numerical results of alignment relaxation, is that a director whose tip lies in the R^- regions, samples extensional strains (**A:nn** >0), while a director whose tip lies in the R^+ regions, samples compressional strains (**A:nn** <0).

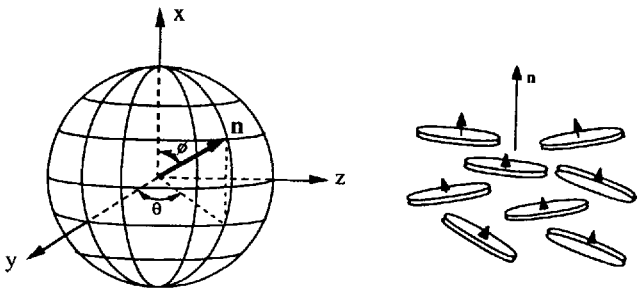

(*a*) (*b*)

Figure 2. Definition of (*a*) coordinate system, and (*b*) director orientation of a uniaxial discotic nematic liquid crystal. (*a*) Director angles and unit sphere: θ $(0\le\theta\le 2\pi)$ is the azimuthal angle and ϕ $(0\le\phi\le\pi)$ is the polar angle. The north pole of the sphere is located at $\phi=0$, the south pole at $\phi=\pi$, and the equator at $(\theta,\phi)=([0,2\pi],\pm\pi/2)$, **n** denotes the director. (*b*) The director in a discotic nematic phase is the average orientation of the unit normals to the disc-like molecules.

2.2. *Governing orientation and alignment equations*

The macroscopic model used in this paper has been described in detail in [22]. Here we just present the governing equations for the temporal evolution of the director field $\mathbf{n}(t)$ and the alignment $S(t)$, and refer the reader to the above mentioned paper for details. The governing equations for our model uniaxial discotic nematics, subjected to a given isothermal flow, are

$$\begin{bmatrix} dn_i/dt \\ dS/dt \end{bmatrix}=\begin{bmatrix} W_{ij}n_i+\lambda(A_{ij}n_j-(A_{lk}n_ln_k)n_i) \\ \beta_1A_{lk}n_ln_k+\beta_2/\tau_1 \end{bmatrix}, \tag{7a, b}$$

where the components of the vorticity tensor **W** are $W_{ij}=(v_{i,j}-v_{j,i})/2$. $\lambda(S)$ is the tumbling function, $\beta_1(S)$ the ordering function, and $\beta_2(S,U)$ is proportional to the thermodynamic driving force; these functions are given by

$$\lambda=-\frac{\gamma_2}{\gamma_1}=-(3\sigma_4^*+\sigma_6^*S)/(3S+\tau_2^*S^2), \tag{8a}$$

$$\beta_1=-(9\sigma_4^*+6\sigma_6^*S)/(6+4\tau_2^*S) \tag{8b}$$

and

$$\beta_2=(-3S+US+US^2-2US^3)/(3+2\tau_2^*S), \tag{8c}$$

where the starred coefficients are scaled with the alignment relaxation time τ_1 that appears in equation (7*b*).

To select numerical values for the three phenomenological parameters σ_4^*, σ_6^*, τ_2^*, we enforce the following constraints on the signs of λ and γ_1 (9–12] and on the values of λ when $S=0$ and $S=1$ [9]

$$\lambda=-\frac{\gamma_2}{\gamma_1}<0;\quad \gamma_1\ge 0;\quad \lim_{S\to 0}\lambda=-\infty;\quad \lim_{S\to 1}\lambda=-1. \tag{9a, b, c, d}$$

The adopted values that satisfy the constraints are: $\sigma_4^*=1/10$, $\sigma_6^*=1{\cdot}7$, $\tau_2^*=-1{\cdot}0$, and the resulting λ and β_1 are shown in figure 3; the relevant phenomena described in this paper are captured by other arbitrary triplets that satisfy equations (9), and the values adopted here were chosen only for convenience. It is worth noting that for

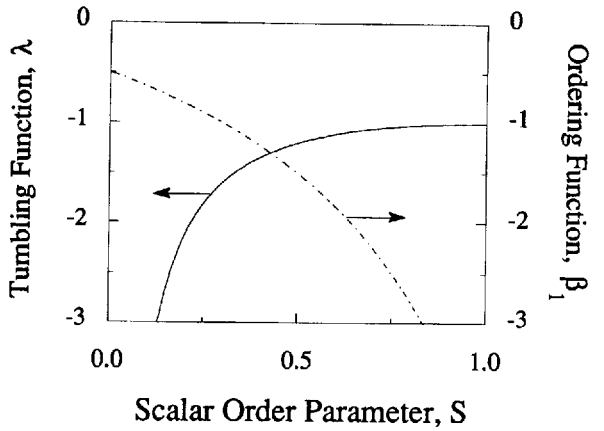

Figure 3. Tumbling function λ and the ordering function β_1 as a function of the scalar order parameter S. The tumbling function is the ratio of the coefficient for strain and vorticity torques, while the ordering function is the coefficient for the ambient strain rate **A**:**nn** that governs the relaxation of S. For discotics (rod-like) nematics both are negative (positive).

extensional flows all steady states are simple fixed points and thus adoption of the different $\lambda(S)$ and $\beta_1(S)$ will only change the time scales but the significant phenomena will be essentially unchanged.

The simplifying assumptions and approximations made in deriving the mathematical model that describes the flow-induced alignment and orientation of an ideal discotic nematic liquid crystal, as given by equations (7) and (8), can be found in [22].

The velocity field $\mathbf{v}(x,y,z)$ corresponding to the extensional start-up flow of the nematic sample, is given by [23]

$$\left.\begin{aligned} &v_x = a\dot{\varepsilon}xH(t); \quad v_y = -a\frac{\dot{\varepsilon}}{2}(1+b)yH(t);\\ &v_z = -a\frac{\dot{\varepsilon}}{2}(1-b)zH(t); \quad H(t)=\begin{cases}0 & t<0\\ 1 & t\geq 0\end{cases}, \end{aligned}\right\} \quad (10\,a,b,c,d)$$

where $\dot{\varepsilon}$ is the given constant extension rate. The corresponding rate of deformation tensor **A**, is given as

$$\mathbf{A}=\dot{\varepsilon}\begin{bmatrix} a & 0 & 0\\ 0 & -\frac{a}{2}(1+b) & 0\\ 0 & 0 & -\frac{a}{2}(1-b)\end{bmatrix}, \quad (11)$$

where $a=+1$ or -1, and $0\leq b\leq 1$ captures the range of possible extensional flows. Uniaxial extensional flow (UE) is given by $a=+1$, $b=0$, biaxial extensional flow (BE) by $a=-1$, $b=0$, and planar extensional flow (PE) by $a=+1$, $b=+1$. These flows are irrotational and the vorticity tensor is zero ($\mathbf{W}=\mathbf{0}$). Replacing equations (10) and (11) in equations (7), the following set of coupled non-linear ordinary differential equations for extensional isothermal, incompressible flows of uniaxial discotic nematic crystals are obtained:

$$\frac{dn_x}{d\varepsilon}=\frac{a}{2}\lambda[3(1-n_x^2)+(n_y^2-n_z^2)]n_x, \quad (12\,a)$$

$$\frac{dn_y}{d\varepsilon}=-\frac{a}{2}\lambda[3n_x^2+b(1-n_y^2+n_z^2)]n_y, \quad (12\,b)$$

$$\frac{dn_z}{d\varepsilon}=-\frac{a}{2}\lambda[3n_x^2-b(1+n_y^2-n_z^2)]n_z, \quad (12\,c)$$

and

$$\frac{dS}{d\varepsilon}=\frac{a}{2}\beta_1[3(n_x^2-1)-b(n_y^2-n_z^2)]n_z+\mathrm{De}^{-1}\beta_2 \quad (12\,d)$$

where $\varepsilon=\dot{\varepsilon}t$ is the strain (dimensionless time), $\mathrm{De}=\dot{\varepsilon}\tau_1$ is the alignment Deborah number (dimensionless strain rate). We note that equations (12) are dimensionless, and thus, for a given set of parameters, the solution vector (S, **n**) is only a function of the strain (dimensionless time) $\varepsilon=\dot{\varepsilon}t$. In the absence of Frank elasticity [15], strain scaling is typical of liquid crystalline flow phenomena [31]. When $\mathrm{De}\to 0$ the alignment (S) relaxation is elastic, when $\mathrm{De}\to\infty$ it is purely viscous, and for the intermediate values it is viscoelastic. At intermediate De the director relaxation is also viscoelastic, since it is coupled to S through $\lambda(S)$.

The initial conditions used to solve equations (12) are

$$@\varepsilon=0:\ \mathbf{n}=\mathbf{n}_o;\quad S=S_{eq};\quad \mathbf{n}_o\cdot\mathbf{n}_o=1 \quad (13)$$

where $S_{eq}(U)$ is the equilibrium scalar order parameter of the normal ($S>0$) uniaxial nematic phase, found by setting the numerator of equation (8 c) equal to zero [32]

$$S_{eq}=\frac{1}{4}+\frac{3}{4}\sqrt{\left(1-\frac{8}{3U}\right)}. \quad (14)$$

For $U<8/3$ the stable phase is isotropic, for $8/3\leq U\leq 3$ there is biphasic equilibrium. In this paper we use two representative nematic potentials $U=3$ and $U=5$, and the corresponding initial conditions are: $S_{eq}\,(U=3)=0{\cdot}5$ and $S_{eq}\,(U=5)=0{\cdot}76$. All angles are reported in degrees.

Equations (12) are integrated using an implicit corrector-predictor first order Euler integration method with an adaptable time step [33]. Application of the implicit corrector-predictor method transforms the set of coupled nonlinear ordinary differential equations (12) into a set of coupled nonlinear algebraic equations. For each time step the algebraic equations are solved using the Newton–Raphson iteration scheme [33]; the predictor step generates a first guess for the iteration loop and the corrector step is the iteration loop itself. The adopted convergence criteria is that the length of the difference

vector between the calculated solution vectors corresponding to two successive iterations is less than 10^{-6}. The transient solution vector obtained from the numerical solutions ($\mathbf{n}(\varepsilon)$, $S(\varepsilon)$), is used to calculate the tensor order parameter $\mathbf{Q}(\varepsilon)$, and the converged steady state solutions ($\mathbf{n}_{SS}$, S_{SS}) are used to compute the steady flow birefringence. To facilitate the discussion and perform an analysis of the numerical solutions, some of the computed results are presented in reference to the unit sphere description of the director field.

3. Analytical results

3.1. *Director dynamics*

Integration of the set of equations (12) yields, with **A** given by equation (11), the following expression for the director relaxation $\mathbf{n}(\varepsilon)$ for any extensional start-up flow

$$\left.\begin{aligned} n_i(\varepsilon)&=\frac{E_{ij}n_{jo}}{|\mathbf{E}.\mathbf{n}_o|};\quad n_i(0)=n_{io};\\ E_{ij}(\varepsilon)&=\exp\left\{\tilde{A}_{ij}\int_0^{\varepsilon}\lambda d\varepsilon'\right\};\quad \tilde{A}_{ij}=A_{ij}/\dot{\varepsilon}, \end{aligned}\right\} \quad (15a,b,c,d)$$

and in the component form

$$n_x=\frac{E_{xx}n_{xo}}{|\mathbf{E}.\mathbf{n}_o|};\quad n_y=\frac{E_{yy}n_{yo}}{|\mathbf{E}.\mathbf{n}_o|};\quad n_z=\frac{E_{zz}n_{zo}}{|\mathbf{E}.\mathbf{n}_o|}, \quad (16a,b,c)$$

$$E_{xx}=\exp\left(a\int_0^{\varepsilon}\lambda d\varepsilon'\right), \quad (16d)$$

$$E_{yy}=\exp\left(-\frac{1}{2}a(1+b)\int_0^{\varepsilon}\lambda\, d\varepsilon'\right), \quad (16e)$$

$$E_{zz}=\exp\left(-\frac{1}{2}a(1-b)\int_0^{\varepsilon}\lambda\, d\varepsilon'\right), \quad (16f)$$

and

$$E_{ij}=0 \text{ for } i\neq j \quad (16g)$$

where n_{jo} is the jth component of the initial director orientation ($\mathbf{n}(0)$). Figure 4 shows representative computed director trajectories for uniaxial extension, biaxial extensional and planar extensional flows projected onto the y–z plane, here the x axis is normal to the plane of the paper, and the direction of the director paths are indicated by the direction of arrows. The figure shows that for uniaxial extensional and biaxial extensional flows the director follows identical paths but in reverse directions. In terms of the adopted polar (ϕ) and azimuthal (θ) angles, the director trajectories, given by equations (16), are as follows

Uniaxial extensional flow:

$$\tan(\theta)=1/d_1;\quad 0\leq\phi\leq\pi;\quad -\infty<d_1<\infty, \quad (17a)$$

Biaxial extensional flow:

$$\tan(\theta)=1/d_1;\quad 0\leq\phi\leq\pi;\quad -\infty<d_1<\infty \quad (17b)$$

Planar extensional flow:

$$\tan(\theta)\sin(\theta)=1/d_2\cot(\phi);\ 0\leq\phi\leq\pi;\ -\infty<d_2<\infty, \quad (17c)$$

where $d_1=n_y/n_z$, and $d_2=n_xn_y/n_z^2$ for time $t\geq 0$. Comparing equations (5), (6) and (16) it follows that for uniaxial extensional and biaxial extensional flows, the director trajectories belong to the meridians of the unit sphere, and the director dynamics belong to the class of geodesic flows [22]. Equation (17 c) and figure 4 show that planar extensional flow is not a geodesic flow, except when $d_2\to\infty$ ($\mathbf{n}_o$ lying along the x–y plane or the y–z plane); in practice due to the presence of the fluctuations this exceptional case will not occur. The director trajectories should exhibit the characteristic sensitive dependence on initial conditions which is typical of geodesic flows [34] or of arbitrary flows on a sphere with multiple fixed points.

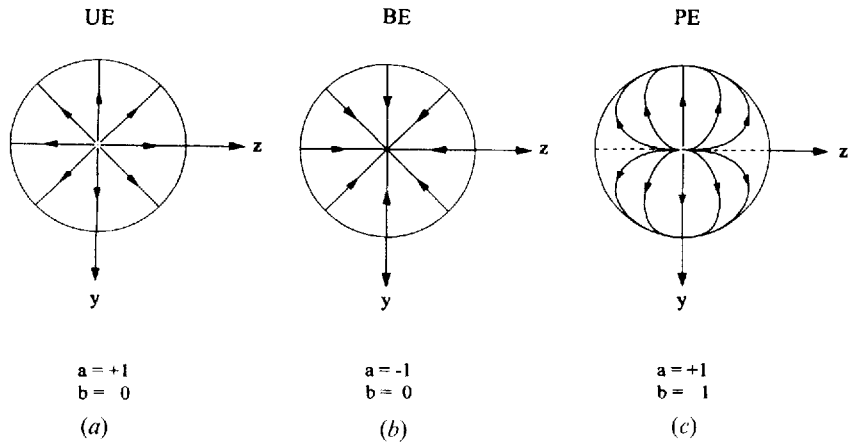

Figure 4. Schematics of the director trajectories on the y–z plane for (*a*) uniaxial extensional flow (UE), (*b*) biaxial extensional flow (BE), and (*c*) planar extensional flow (PE). For uniaxial (biaxial) extensional flow the sources are the poles (equator) and the sink is the equator (poles). For planar extensional flow the sources are the poles and the sinks are $n_y=\pm 1$.

Table 1. Steady states and sensitive initial conditions of the director.

Flow type		Strongest compression direction	Director steady states			Sensitive dependence to initial conditions
			n_{xss}	n_{yss}	n_{zss}	
$a=+1$	$b=0$	y-z plane	0	$\frac{\pm n_{yo}}{\sqrt{(1-n_{xo}^2)}}$	$\frac{\pm n_{zo}}{\sqrt{(1-n_{xo}^2)}}$	$n_{xo}=\pm 1$
$a=+1$	$0<b\leq 1$	y axis	0	± 1	0	$n_{yo}=0$
$a=-1$	$0\leq b\leq 1$	x axis	± 1	0	0	$n_{xo}=0$

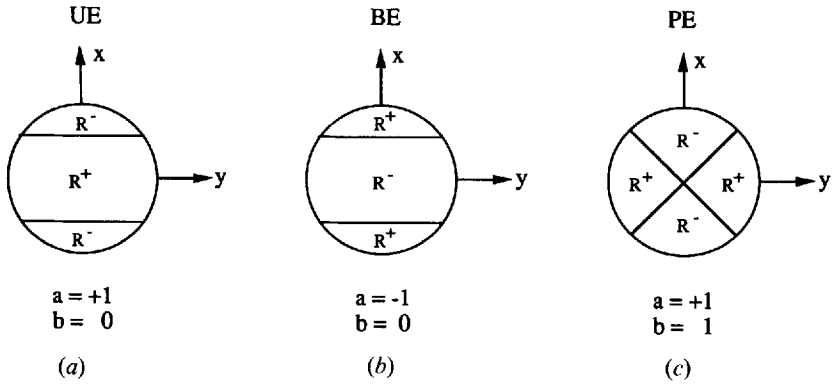

Figure 5. Sensitivity of the initial alignment S relaxation to the initial director orientation. The different characteristic regions for the ambient strain rate **A:nn** for (*a*) uniaxial extensional flow (UE), (*b*) biaxial extensional flow (BE), and (*c*) planar extensional flow (PE). In the R^- regions the alignment rate is positive (**A:nn**>0), and in the R^+ regions the alignment rate is negative (**A:nn**<0).

The sensitive dependence on initial conditions for each extensional flow type are

Uniaxial extensional flow:

$$n_{xo}=\pm 1, \tag{18a}$$

Biaxial extensional flow:

$$n_{xo}=0 \tag{18b}$$

Planar extensional flow:

$$n_{yo}=0. \tag{18c}$$

When the initial director orientation for each flow type is along those defined in equations (18) predictability is lost; for example, in planar extensional flow, if $n_{yo}=0$ the director may evolve with equal likelihood towards the positive y axis or towards the negative y axis. Table 1 summarizes the relations between flow types ($a=\pm 1$, $0\leq b\leq 1$), the compression direction or compression plane, and the stable steady state director orientations. The entries in table 1 show that for all cases the director always aligns along the compression direction or the compression plane of the flow. It is worth noting that when $a=-1$, the stable steady state director orientation is insensitive to the magnitude of b, since for these flows the strongest compression direction always lies along the x axis. On the other hand when $a=+1$, the strongest compression plane changes from the y-z plane when $b=0$, to the y axis when $b\neq 0$. These observations can be used to classify the orienting strength of each extensional flow, since as shown above, the sensitive dependence to initial conditions for biaxial extensional and planar extensional flows leads to no uncertainty (since $\mathbf{n}=-\mathbf{n}$) while for uniaxial extensional flow the magnitude of largest uncertainty is the whole equator ($n_x=0$). Thus, on a relative scale, biaxial extensional and planar extensional flows are strongly orienting flows while uniaxial extensional flow is a weakly orienting flow.

Another important practical property of each flow is the presence or absence of geodesic flow, because this will determine the number of strain units required to achieve the steady director orientation; geodesic flows will, in general, require less strains because a geodesic path is the shortest. For example, figure 4(*c*) shows that for planar extensional flows the paths are generally longer and thus the number of applied strains to achieve steady state must be larger than for the uniaxial extensional and biaxial extensional flows.

3.2. *Alignment dynamics*

The alignment relaxation $S(\varepsilon)$ depends on $\mathbf{n}_0$ through the ambient strain rate **A:nn**. Figure 5 shows different

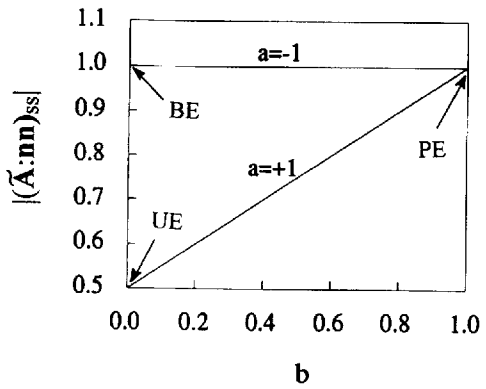

Figure 6. Alignment strength (absolute value of steady state dimensionless ambient strain rate) $|(\tilde{\mathbf{A}}:\mathbf{nn})_{SS}|$ as a function of the flow parameter b, for all types of extensional flows. The biaxial extensional and planar extensional flows are more strongly aligning than uniaxial extensional flow.

representative regions for **A:nn**: in the R^- regions the ambient strain rate is positive (**A:nn** >0), and in the R^+ regions the ambient strain rate is negative (**A:nn** <0). The initial alignment relaxation characteristics are given by

$$\left.\begin{aligned} &\mathbf{n}_o \text{ in } R^-: \left(\frac{dS}{d\varepsilon}\right)_{\varepsilon=0^+} < 0; \\ &\mathbf{n}_o \text{ in } R^+: \left(\frac{dS}{d\varepsilon}\right)_{\varepsilon=0^+} > 0; \\ &\mathbf{n}_o \text{ in } \partial R^- = \partial R^+: \left(\frac{dS}{d\varepsilon}\right)_{\varepsilon=0^+} = 0. \end{aligned}\right\} \quad (19\,a,b,c)$$

It follows from equations (19) that for any De, a sufficient condition for increasing S is that $\mathbf{n}_o$ is in R^+. For large De, discotic nematics, initially in R^-, undergo a temporary melting while the director is in region R^- [22].

In case of polymer flows [8] a flow type may be characterized as weakly aligning or strongly aligning depending on the degree of alignment change in the flowing units. In the present case, our model predicts that the alignment strength is directly proportional to $|(\tilde{\mathbf{A}}:\mathbf{nn})_{SS}|$. Figure 6 shows the dimensionless steady state alignment strength $|(\tilde{\mathbf{A}}:\mathbf{nn})_{SS}|$ for all the possible extensional flows ($a=\pm 1, 0\le b\le 1$). The figure clearly shows that when $a=-1$ the alignment strength is insensitive to the magnitude of b, but for $a=+1$, it is highly sensitive to the value b. The figure also shows the location of the three representative extensional flows. Table 2 shows the relations between the flow aligning strength and the flow parameters a and b, for general extensional flows. Comparing the various entries in table 2, it follows that the highest flow alignment strength scales with the strongest compressional strains ($a=-1, 0\le b\le 1$; and $a=1$, $b=1$) as in biaxial extensional and planar extensional flows, while the lowest alignment strength scales with the weakest compressional strains ($a=+1$, $b=0$) as in uniaxial extensional flow.

Table 2. Alignment strength of extensional flows.

Flow type		Alignment strength $\lvert(\tilde{\mathbf{A}}:\mathbf{nn})_{SS}\rvert$
$a=+1$	$b=0$	$\frac{1}{2}$
$a=+1$	$0<b\le 1$	$\frac{1}{2}(1+b)$
$a=-1$	$0\le b\le 1$	1

4. Numerical results

4.1. *Orientational relaxation*

Figure 7 (a) ahows the director orientation relaxation, in terms of the azimuthal director angle θ and the polar director angle ϕ as a function of strain (dimensionless time) $\varepsilon=\dot{\varepsilon}t$, for uniaxial extensional flow (solid line), biaxial extensional flow (dot-dash line), and planar extensional flow (triple dot-dash line), for De $=0{\cdot}5$, $U=5$, and with the initial director orientation $(\theta_o,\phi_o)=45,45)$. Figure 7 (b) shows the corresponding computed scientific visualization of the director relaxation, represented by the normals to the shown discs. Figure 7 (a) shows that for uniaxial extensional flow the steady director orientation is $(\theta_{SS},\phi_{SS})=(45,90)$, for biaxial extensional flow it is $(\theta_{SS},\phi_{SS})=(45,0)$, and for planar extensional flow it is $(\theta_{SS},\phi_{SS})=(0,90)$, in agreement with the predictions summarized in table 1. The visualization in figure 7 (b) shows that the director exhibits different combinations of twisting and tilting as the strain increases but that the final steady state orientation is always along the strongest compression direction(s) for each flow. It can be shown that for all extensional flows, the director relaxation is faster at higher De and at lower U, since for these conditions the adapted $\lambda(S)$ samples larger absolute values.

Figure 8 shows the x and z components of the director as a function of strain (dimensionless time) $\varepsilon=\dot{\varepsilon}t$, for uniaxial extensional flow (solid line) and planar extensional flow (dot dash line), for De $=0{\cdot}5$, $U=5$, and with the initial director orientation $(n_{xo}=0{\cdot}9990,\ n_{yo}=0{\cdot}0004,\ n_{zo}=0{\cdot}0447)$ or $(\theta_o,\phi_o)=(89{\cdot}4, 2{\cdot}56)$. The figure shows that the number of strain (dimensionless time) units required to achieve steady state director orientation for planar extensional flow is considerably larger than those for uniaxial extensional flow. For the selected $\mathbf{n}_o$, the director follows, in both cases, a trajectory close to the x-z plane till the equator is reached; this is the reason for the comparable n_x dynamics in both the cases. The main difference in required strains arises from the fact that for

planar extensional flow only the y axis is the compression direction, and thus n_z must now decay to zero.

4.2. *Alignment viscoelastic relaxation*

Figure 9 shows the alignment relaxation $S(\varepsilon)$ for uniaxial extensional flow (solid line), biaxial extensional flow (dash-dot line), and planar extensional flow (triple dot-dash line) corresponding to the initial director orientation of figure 7, and for (*a*) $U=5$, De$=0{\cdot}5$, (*b*) $U=5$, De$=0{\cdot}1$, (*c*) $U=3$, De$=0{\cdot}5$, and (*d*) $U=3$, De$=0{\cdot}1$. The

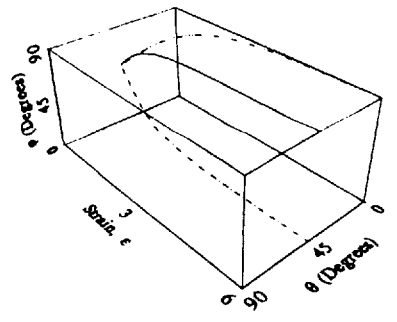

(*a*)

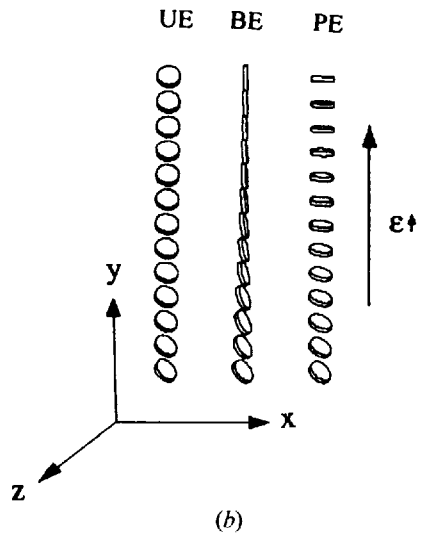

(*b*)

Figure 7. (*a*) Aximuthal director angle θ and polar director angle ϕ as a function of strain (dimensionless time) $\varepsilon=\dot{\varepsilon}t$, for uniaxial extensional flow (solid line), biaxial extensional flow (dot-dash line), and planar extensional flow (triple dot-dash line) for De$=0{\cdot}5$, $U=5$, and initial director orientation $(\theta_o, \phi_o)=(45, 45)$. The figure shows the orientation relaxation of the director for three different types of extensional flows. (*b*) Corresponding computed scientific visualization of the director relaxation, represented by the normals to the shown discs. For the same initial orientation, the steady state director orientation is different and the final steady state depends on the type of extensional flow.

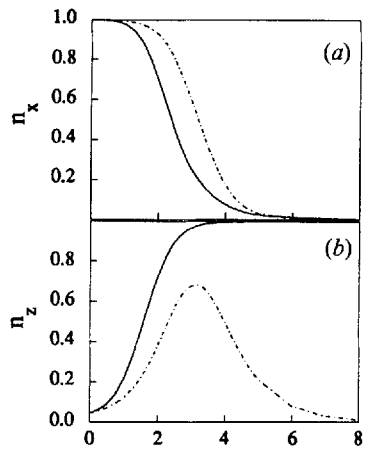

Figure 8. Director components as a function of strain (dimensionless time) $\varepsilon=\dot{\varepsilon}t$, for uniaxial extensional flow (solid line) and planar extensional flow (dot-dash line) for De$=0{\cdot}5$, $U=5$, and initial director orientation $(n_{xo}=0{\cdot}9990, n_{yo}=0{\cdot}0004, n_{zo}=0{\cdot}447)$ or $(\theta_o, \phi_o)=(89{\cdot}4, 2{\cdot}56)$. The number of strains (dimensionless time) units required to achieve steady state orientation for planar extensional flow is considerably larger than for uniaxial extensional flow.

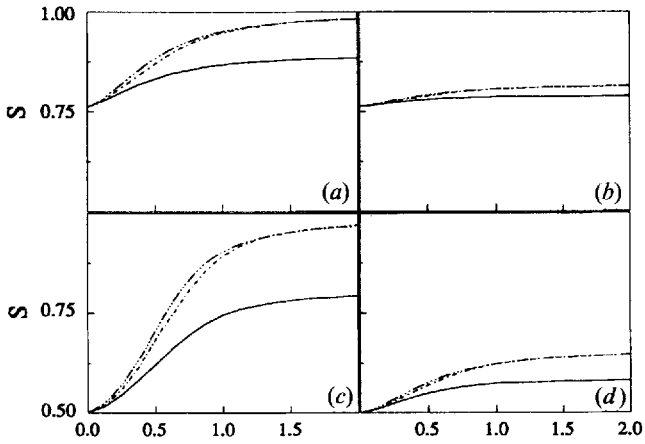

Figure 9. The alignment relaxation S $(\varepsilon=\dot{\varepsilon}t)$ for uniaxial extensional flow (solid line), biaxial extensional flow (dash-dot line), and planar extensional flow (triple dot-dash line) corresponding to the initial director orientation of figure 6, for (*a*) $U=5$, De$=0{\cdot}5$; (*b*) $U=5$, De$=0{\cdot}1$; (*c*) $U=3$, De$=0{\cdot}5$; and (*d*) $U=3$, De$=0{\cdot}1$. Here $\varepsilon=\dot{\varepsilon}t$ denotes strain or dimensionless time. The figure shows that the relaxation is more sensitive to the alignment strength of the flow at higher De (viscous mode) and at lower U (elastic mode).

relaxation coordinate $\varepsilon=\dot{\varepsilon}t$ is the strain (dimensionless time). The figure shows that biaxial extensional and planar extensional flows have similar relaxations and both lead to higher steady state values of the alignment S than in case of uniaxial extensional flow, as predicted in table 2. The figure shows that at higher De, the dynamics of S are slower than at lower De, for both low and high values of U, and that this trend is independent of the flow type. In addition at higher De, the viscous mode dominates the viscoelastic relaxation at all the times, and the effect of the relative magnitude of U is smaller, while at lower De, the elastic mode dominates and the effect of U is larger. It also follows from the figure that at higher De, the dynamics and steady state value of S is more sensitive to the value of U in the case of uniaxial extensional flow than in case of biaxial extensional and planar extensional flows, because at a given De, the flow alignment strength ($|(\tilde{\mathbf{A}}:\mathbf{nn})_{SS}|$) in the former is lower than in the last two cases. At lower De, the flow-type sensitivity is weaker since in this regime the elastic mode dominates.

4.3. *Tensor order parameter relaxation and flow birefringence*

Figure 10 shows the relaxation of the components of the tensor order parameter $\mathbf{Q}$ as a function of strain (dimensionless time) $\varepsilon=\dot{\varepsilon}t$ with initial director orientation $(\theta_o, \phi_o)=(45, 45)$, for $U=3$ and $De=0{\cdot}5$, and for (*a*) uniaxial extensional flow (solid line), (*b*) biaxial extensional flow (dash–dot line), and (*c*) planar extensional flow (triple dash–dot line). For the shown parameters the relaxation is virtually complete after 5 strain (dimensionless time) units. The trace elements of $\mathbf{Q}$ scale with the alignment strength of the flow and the relative orientation between n_{SS} and compression directions of $\mathbf{A}$. A summary of the main features of the steady state values of trace of $\mathbf{Q}$ is as follows:

Q_{yy}: The biaxial extensional flow exhibits the lowest value since n_y is normal to the compression axis (x axis) while the planar extensional flow attains the highest magnitude since n_y is along the compression axis (y axis) and the alignment strength is high.

Q_{xx}: Since n_x is normal to the extension direction for uniaxial extensional and planar extensional flows, thus Q_{xx} is small, while for biaxial extensional flow, the net combination due to the fact that n_x is along the compressional axis and that the high alignment strength gives a relative large Q_{xx}.

Q_{zz}: Here the compression directions for biaxial extensional and planar extensional flows are orthogonal to n_z and thus for these flows Q_{zz} is small. For uniaxial extensional flow, although n_z lies in the compressional plane the weakly aligning character of the flow yields a relatively low Q_{zz}.

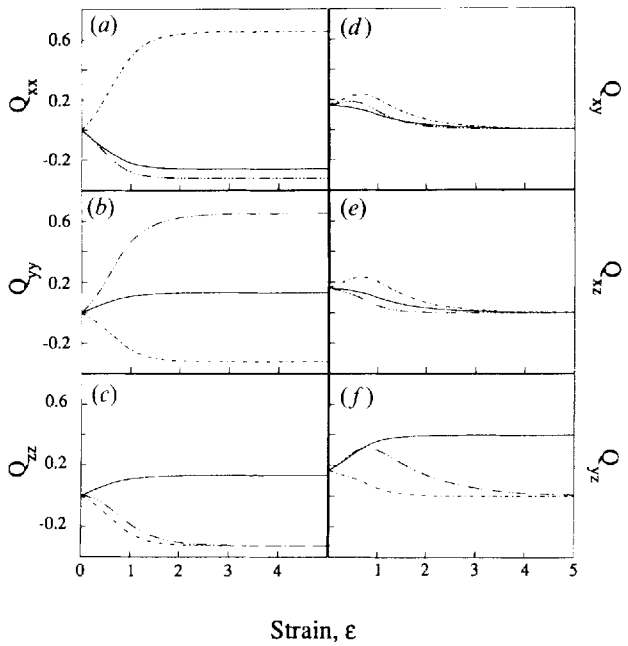

Figure 10. The relaxation of the components of the tensor order parameter $\mathbf{Q}$ ($\varepsilon=\dot{\varepsilon}t$) with initial director orientation $(\theta_o, \phi_o)=(45, 45)$, for $U=3$ and $De=0{\cdot}5$, and for (*a*) uniaxial extensional flow (solid line), (*b*) biaxial extensional flow (dash–dot line), and (*c*) planar extensional flow (triple dash–dot line). The relaxation coordinate $\varepsilon=\dot{\varepsilon}t$ is the strain or dimensionless time. The magnitude of the different components scale with the alignment strength of each flow, and with the relative orientations between the different elements of $\mathbf{Q}$ and the compression directions of each flow.

The steady state values of the off-diagonal components ($Q_{ij}, i\neq j$) are equally explained by taking into account the alignment strength of the flow and the compression directions of the flow. For example Q_{yz} vanishes for biaxial extensional and planar extensional flows since n_z is parallel to the compression direction of these flows, while for uniaxial extensional flow Q_{yz} is relatively large since n_y and n_z are both in the compression plane of the flow.

According to [26], the birefringence $\Delta\eta$ can be expressed by

$$\Delta\eta=\sqrt{e_{\parallel}}-\sqrt{e_{\perp}}\approx\frac{\Delta e_{max}S}{2\sqrt{\tilde{e}}}, \tag{20}$$

where $e_{\parallel}$ and $e_{\perp}$ are the elements of the dielectric tensor e_{ij} parallel and normal to the director, respectively, the tensor e_{ij} is given by $e_{ij}=\tilde{e}\delta_{ij}+\Delta e_{max}Q_{ij}$, where the first term is the average trace of e_{ij} and Δe_{max} is the anisotropy for $S=1$; for discotics, $\Delta\eta<0$ since $\Delta e_{max}<0$. In deriving equation (20) we have assumed that $\tilde{e}\gg 2\Delta e_{max}S/3$ for the

values of S corresponding to the nematic phase. Equation (20) shows that the steady flow-induced birefringence $\Delta\eta_{SS}$ is proportional to the magnitude of the steady alignment S_{SS}.

Figure 11 shows the steady state alignment S_{SS} as a function of De for uniaxial extensional flow (solid line), for biaxial extensional and planar extensional flows (dash-dot line) for (*a*) $U=5$, and (*b*) $U=3$. As shown in table 2, the alignment strength of biaxial extensional and planar extensional flows is identical and thus the shown curve for these two flows superpose. The figure shows a monotonic increase in the flow birefringence. At high De the viscous mode dominates and the effect of the magnitude of U is smaller, while at low De the elastic mode dominates and the effect of the magnitude of U on S_{SS} is larger irrespective of the flow type. The figure shows, in agreement with table 2, that the birefringence for uniaxial extensional flow is smaller than for other flow types since it is a weakly aligning flow. The alignment strength of each flow type explains the relative sensitivity of the birefringence to De for the various flows. At higher U the effect due to the different alignment strengths is smaller than at lower U. At lower U, the viscous mode dominates and the effect due to the different degrees of alignment strengths increases rapidly with increasing De.

4. Conclusions

In this initial investigation of the nematorheology of uniaxial discotics in extensional flows, we have performed a useful characterization of the sensitivity of the director, scalar order parameter, and tensor order parameter relaxation with respect to the flow type, the alignment Deborah number, and the initial director orientation. Use of the unit sphere description identified the director dynamics of uniaxial extensional and biaxial extensional flows as geodesic flows, and as non-geodesic (except for one special case) for planar extensional flow. The three flows exhibit sensitive dependence to initial conditions, but due to the double arrow nature of the director vector ($\mathbf{n}=-\mathbf{n}$,) biaxial extensional and planar extensional flows are strongly orienting flows since they have one stable fixed point. On the other hand, uniaxial extensional flow is a weakly orienting flow, since the stable steady states are a degenerate circle, and when $\mathbf{n}_0$ is on the poles of the unit sphere, predictability is lost. Significant differences between flow types arise in the number of strain units required to achieve steady state orientations, according to whether the flow is geodesic (uniaxial extensional or biaxial extensional flows) or non-geodesic (planar extensional flow). The alignment strength ($|(\tilde{\mathbf{A}}:\mathbf{nn})_{SS}|$) of the flows scale with the magnitude of the ambient strain rate ($\mathbf{A}:\mathbf{nn}$). It is found that uniaxial extensional flow is a weakly aligning flow but biaxial extensional and planar extensional flows are strongly aligning flows. A summary of the aligning and orienting properties, and of the geometry of the director orbits of the main extensional flows, is given in table 3.

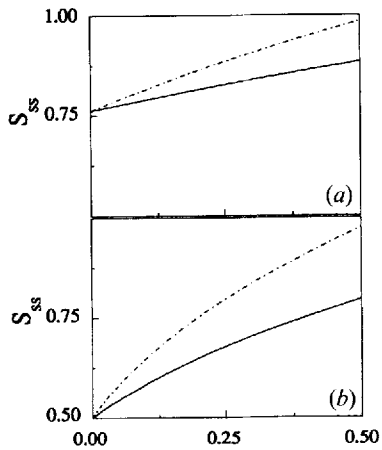

Figure 11. The steady state alignment S_{SS} as a function of De for uniaxial extensional flow (solid line), and for both biaxial extensional and planar extensional flows (dash-dot line), for (*a*) $U=5$, and (*b*) $U=3$. The flow birefringence is proportional to S_{SS} and increases with De. The birefringence for biaxial extensional and planar extension flows is identical and is greater than for uniaxial extensional flow for all U and De.

Table 3. Classification of extensional flows.

Flow type	Orientation strength (director)	Alignment strength (scalar order parameter)	Geodesic flow
Uniaxial Extensional flow	Weaker	Weaker	Yes
Biaxial extensional flow	Stronger	Stronger	Yes
Planar extensional flow	Stronger	Stronger	No

This work is supported by a grant from the Natural Sciences and Engineering Research Council of Canada.

References

[1] Gasparoux, H., 1981, *Molec. Crystals liq. Crystals*, **63**, 231.
[2] Otani, S., 1981, *Molec. Crystals liq. Crystals*, **63**, 249.
[3] Zimmer, J. E., and White, J. L., 1982, *Advances in Liquid Crystals*, Vol. 5, edited by H. G. Brown (Academic Press).
[4] Chandrashekhar, S., 1981, *Molec. Crystals liq. Crystals*, **63**, 171.

[5] DESTRADE, C., TINH, N. H., GASPAROUX, H., MALTHÊTE, J., and LEVELUT, A. M., 1981, *Molec. Crystals liq. Crystals*, **71,** 111.
[6] SINGER, L. S., 1985, *Faraday Discuss. Chem. Soc.*, **73,** 265.
[7] TADMOR, Z., and GOGOS, R. G., 1979, *Principles of Polymer Processing* (John Wiley and Sons).
[8] LARSON, R. G., 1988, *Constitutive Equations for Polymer Melts and Solutions* (Butterworths).
[9] VOLOVIK, G. E., 1980, *JETP Lett.*, **31,** 273.
[10] CARLSSON, T., 1982, *Molec. Crystals liq. Crystals*, **89,** 57.
[11] CARLSSON, T., 1983, *J. Phys. Paris*, **44,** 909.
[12] BAALS, H., and HESS, S., 1988, *Z. Naturf.* (*a*), **43,** 662.
[13] HO, A. S. K., and REY, A. D., 1991, *Rheol. Acta*, **30,** 77.
[14] LESLIE, F. M., 1981, *Advances in Liquid Crystals*, Vol. 4, edited by H. G. Brown (Academic Press), pp. 1–81.
[15] DE GENNES, P. G., 1975, *The Physics of Liquid Crystals* (Oxford University Press), pp. 153–165.
[16] ERICKSEN, J. L., 1989, *Liquid Crystals with Variable Degree of Orientation, IMA Preprint Series*, **559.**
[17] IMURA, H., and OKANO, K., 1972, *Jap. J. appl. Phys.*, **11,** 1440.
[18] DIOGO, A. C., and MARTINS, A. F., 1982, *J. Phys., Paris*, **43,** 779.
[19] EDWARDS, B. J., BERIS, A. N., and GRMELA, M., 1991, *Molec. Crystals liq. Crystals*, **201,** 51.
[20] FARHOUDI, Y., and REY, A. D., 1993, *J. Rheol.*, **37,** 289.
[21] MARRUCCI, G., 1991, *Liquid Crystallinity in Polymers*, edited by A. Ciferri (VCH Publishers), pp. 395–423.
[22] SINGH, A. P., and REY, A. D., 1994, *J. Phys. II, France*, **4,** 645.
[23] BIRD, R., ARMSTRONG, R. C., and HASSAGER, O., 1987, *Dynamics of Polymeric Liquids* (Wiley).
[24] BARNES, H. A., HUTTON, J. F., and WALTERS, K., 1989, *An Introduction to Rheology* (Elsevier), p. 75.
[25] PETRIE, C. J. S., 1979, *Elongational Flows* (Pitman).
[26] GRAMSBERGEN, E. F., LONGA, L., and DE JEU, W. H., 1986, *Phys. Rep.*, **135,** 195.
[27] THURSTON, R. N., 1981, *J. Phys., Paris*, **42,** 413.
[28] THURSTON, R. N., 1981, *J. appl. Phys.*, **52,** 3040.
[29] CARLSSON, T., 1986, *Phys. Rev.* A, **34,** 3393.
[30] WEINSTOCK, R., 1954, *Calculus of Variations* (McGraw-Hill), pp. 26–28.
[31] HAN, W. H., and REY, A. D., 1994, *Phys. Rev.* E, **49,** 597.
[32] DOI, M., and EDWARDS, S. F., 1986, *The Theory of Polymer Dynamics* (Oxford University Press), pp. 358–362.
[33] FINLAYSON, B. A., 1986, *Nonlinear Analysis in Chemical Engineering* (McGraw-Hill), pp. 28–31.
[34] RUELLE, D., 1991, *Chance and Chaos* (Princeton University Press), p. 47.